An innovative approach to recovery of fluctuating industrial exhaust heat sources using cascade Rankine cycle and two-stage accumulators

Pengcheng Li[a, c], Qing Cao[d], Jing Li[b,*], Haiwei Lin[a], Yandong Wang[e], Guangtao Gao[f], Gang Pei[g], Desuan Jie[a], Xunfen Liu[a]

[a]*School of Automobile and Traffic Engineering, Hefei University of Technology, 193 Tunxi Road, Hefei, China*

[b]*Research Center for Sustainable Energy Technologies, Energy and Environment Institute, University of Hull, Hull, HU6 7RX, UK*

[c]*DONGFANG ELECTRIC Dongfang Boiler Group CO., LTD., 150 Huangjue Ping, Wuxing Street, Zigong, China*

[d]*School of Mechanical Engineering, Hefei University of Technology, 193 Tunxi Road, Hefei, China*

[e]*Hefei General Machinery Research Institute, 888 Changjiang Road ,Hefei, China*

[f]*China Electronics Technology Group Corp 38th Research Institute, Hefei, China*

[g]*Department of Thermal Science and Energy Engineering, University of Science and Technology of China, 96 Jinzhai Road ,Hefei, China*

Abstract：The fluctuating property of the heat source is a technical obstacle of waste heat recovery, which leads to part-load operation and reduced economics. This work presents a novel system to mitigate the fluctuations by using steam-organic Rankine cycles (RC-ORC) and two-stage steam accumulators. The system can switch between isothermal heat storage and discharge simply by the regulation of water mass flow (m_2) from the low-temperature

accumulator (LTA) to the high-temperature accumulator (HTA). In the heat charge mode, m_2 rises when the inlet temperature or mass flow of the heat source increases. The water level of the HTA elevates. Analogously, in the heat discharge mode, m_2 decreases and more water accumulates in the LTA. The RC-ORC operates under the rated condition consistently through the unique structural design. The fundamentals and features of the system are illustrated. Given two typical heat source conditions, the fluctuations in thermal efficiencies are minor (15.63-15.84% and 19.57-19.70%). Thermo-economic estimation of the tanks indicates that the steel cost is roughly 1306 $ and 432 $, respectively. Compared with the single-stage ORC using stream control, the normalized investment cost (NIC) is reduced by 888-925 $/kW.

Keywords: Steam-organic Rankine cycles; Fluctuating waste heat; Two-stage steam accumulators; Heat storage; Heat discharge

*Corresponding author. Tel./Fax: +44 (0)1482 463611. E-mail: Jing.Li@Hull.ac.uk

1. Introduction

Among the numerous waste heat recovery power generation options, the organic Rankine cycle (ORC) is a proven and widespread technique [1, 2]. However, one of the most critical barriers that limit its implementation is the fluctuating and/or intermittent nature of the heat source, which is common in energy-intensive industries [3]. ORC system is usually designed at the nominal condition when the components like expander, pump and heat exchangers operate at maximum efficiencies. The corresponding optimal heat to power conversion efficiency can be achieved. Nevertheless, the fluctuations lead to part-load operation of the components and performance degradation of the whole system [4]. Furthermore, when

subjected to remarkable fluctuations, the waste heat source may have to be completely by-passed due to the extreme off-design conditions. All these aspects result in prolonged payback time and reduced economic feasibility [1].

Different approaches are adopted to reduce the detrimental effect of the thermal power undulations. These can be classified into two categories: stream control and thermal energy storage (TES). The stream control can ensure 1) the working fluid is fully vaporized before the expander so that it will not get damaged by liquid droplets; 2) the organic fluid does not get overheated which can lead to chemical decomposition. Examples of different stream control configurations are graphed in Fig. 1. Mazzi et al. proposed intermediary thermal oil stream control of flow entering different sections of waste heat boiler (Fig. 1 (a)) [5]. Peralez et al. presented a by-pass valve that controlled exhaust gases entering the waste heat boiler (Fig. 1 (b)) [6]. Pili et al. developed the mixture of ambient cold air with the hot off-gas by a mixing valve (Fig. 1 (c)), where the ambient air was mixed in the incoming hot off-gas before entering the waste heat boiler [7]. The working fluid stream in the evaporator (waste heat boiler) could be controlled with a variable speed pump to match the fluctuations in the available thermal power. A by-pass before the expander was also integrated to protect the turbine from liquid droplets when the fluid was not fully evaporated (Fig. 1 (d)) [8].

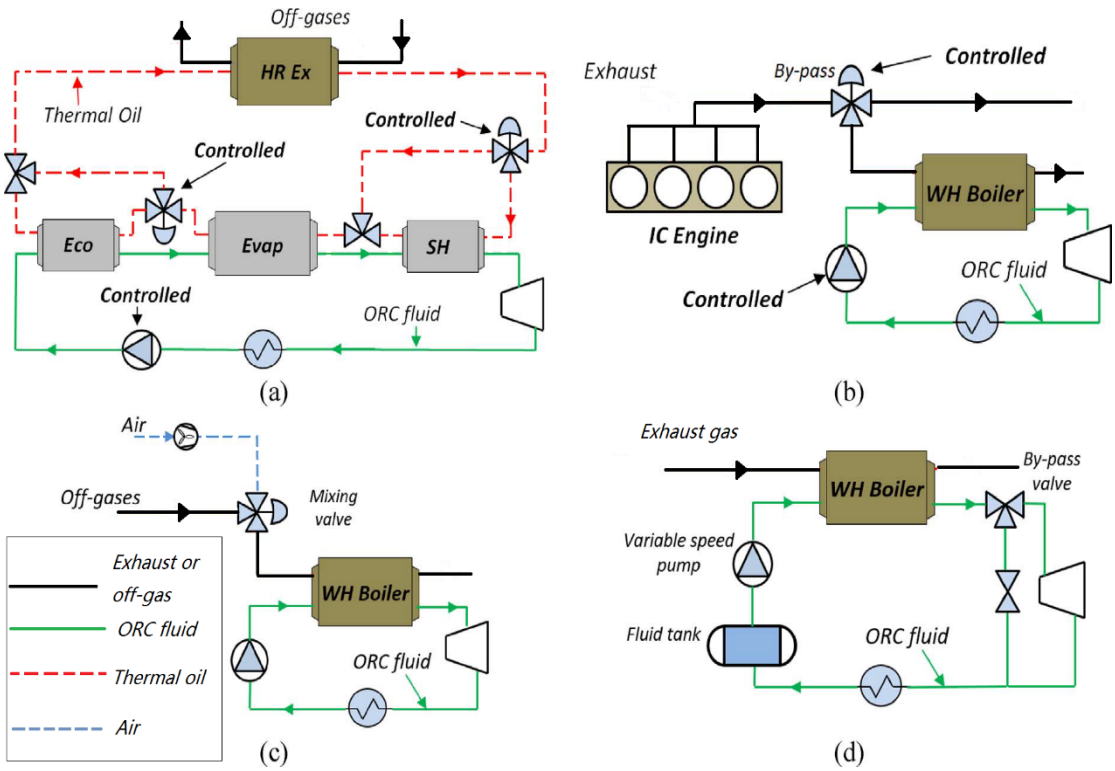

Fig. 1. Examples of stream control configurations.

However, the stream control can only guarantee stable operation when the heat supplied by the hot reservoir equals or exceeds the heat required at the rated condition. There will be a waste of exergy when the heat source energy outstrips the demand. On the contrary, the system will work at the part-load condition or shut down as no heat storage device is installed when the available heat is lower than the design value.

Another solution to mitigate the detrimental impact is TES, which can be divided into sensible and latent heat storage. Thermal oil, molten salts, concrete and steam are representative sensible heat storage media. Steam accumulators produce steam through flashing (known as Ruths storage). Short reaction time and high discharge rate make them a promising option for compensation of fast transients in insolation [9]. Nitrate salts (60% $NaNO_3$ + 40% KNO_3) dual-tank configuration is adopted in the Solar Two [10], Gemasolar plant [11] and Shouhang's 10 MW demonstration model [12]. These successful applications in solar thermal power plants

provide references for mitigating the fluctuation of cogeneration. For instance: a packed bed storage unit using sand in combination with ORC for the utilization of industrial waste heat [13]; Thermal oil (dibenzyl-toluene) storage coupled ORC for heat recovery from diesel engine [14]; Two-tank (Therminol VP-1/ HITEC®) and single tank (Therminol VP-1) structures in recovering energy from clinker cooling air, flue gas hot reheating furnace and electric arc furnaces employing ORCs. The intermediate oil loop converts source mass flow variations into temperature variations by controlling the oil mass flow [7].

Phase change materials (PCMs) are employed in latent heat storage. They seem more attractive because of the high storage capacity per unit volume with isothermal features during charge/discharge cycles [15]. Applications include: an improved PCM (eutectic alloy Al-12%Si)-based ORC recovering heat system for a billet reheating furnace [16], continuous charge electric arc furnace with scrap preheating and the PCM (aluminum)-based smoothing device [17], PCM (Al-12%Si alloy)-coupled steam generator to produce constant superheated steam in the steel industry [18], and ORC integrated with double latent thermal energy storage evaporators using $LiNO_3$-KCl-$NaNO_3$ for engine waste heat recovery [19].

Surplus energy is stored during peak times and reused when the heat supply is deficient through TES. However, it has inevitable flaws compared with the stream control. First, the heat source temperature driving the power cycle is lower than that of the hot reservoir. It is due to the finite heat transfer temperature difference from the hot reservoir to the TES and vice versa [1]. Second, the low thermal conductivity, the degradation of thermophysical properties and the large investment cost of PCMs are the barriers of its applications. Third, the control strategy for latent heat storage is sophisticated because the controller must be able to switch between charging and discharging modes depending on whether the heat transfer fluid temperature is

higher or lower than the PCM melting temperature [20]. Fourth, the additional enormous volume and the ineffective control of temperature are the prominent drawbacks of sensible heat storage.

In order to reduce the enormous exergy loss in stream control and alleviate the difficulties in TES, this work develops a novel technology of resilient control and cost-effective storage for waste heat recovery to tackle the challenges of fluctuation in heat sources and achieve a good level of thermal efficiency and constant power output. Cascade steam-organic Rankine cycles (RC-ORC) and two-stage steam accumulators are employed for power conversion and thermal storage, respectively. Different from conventional steam accumulators using merely the sensible heat of water, both the latent heat stored in HTA and the sensible heat released from HTA to LTA is employed in the novel system. The former is used to drive the RC-ORC while the latter provides partial heat for the bottom ORC. The Off-design phenomenon caused by the flashing process is avoided due to the constant temperature and pressure in both accumulators. Meanwhile, the system retains the advantages of latent heat storage, but the slow thermal response attributed to the low thermal conductivity of PCM is overcome. Rapid response to the fluctuation and stable power conversion can be realized by controlling the flow of water from the low-temperature accumulator (LTA) to the high-temperature accumulator (HTA). Moreover, a maximum heat recovery ratio and reduced irreversible loss are guaranteed.

To the best of the authors' knowledge, it is the first time that the RC-ORC has been combined with the two-stage accumulators in the waste heat recovery application. The potential of this combination has been explored for the concentrated solar power generation system. It's shown that an increment in storage capacity of about 460% can be achieved [21, 22]. Notably, the characteristics of solar energy resource and industrial waste heat are different. The former is

unavailable at night, while the latter may fluctuate 24 h a day and there is no need to store a large amount of heat during the daytime. Different working principles and control strategies are expected when it comes to waste heat recovery. To this end, a unique operation of the ORC driven parallelly by the top steam Rankine cycle (RC) and accumulators is proposed in this paper.

The operating principles and characteristics are elaborated, followed by thermodynamic property analysis of the system and economic estimation of the tanks in two typical situations. Finally, thermo-economic performance comparison with the traditional single-stage ORC using stream control is executed.

2. Description of the system

2.1 Fundamentals

Fig. 2 illustrates the structure of the innovative system. The line segments of different colors represent the flow process curves of different mass flow rates. The top cycle is the RC, which mainly consists of HTA, evaporator (HX1), screw expander (SE), condenser (HX3), and pump (P1). The bottom cycle is the ORC, which comprises preheater (HX4), dry fluid turbine, condenser (HX5) and pump (P2). The bottom of the HTA is connected with the top of the LTA through HX4 and a sliding sleeve throttle valve.

Following operating principles are summarized.

(1). The mass flow rates of RC and ORC (m_3 and m_4) are kept constant, respectively, as well as the water mass flow rate from HTA to LTA (m_5).

(2). The thermodynamic parameters of points 1~4, 7~11 and 14~18 are fixed.

(3). Combining (1) and (2), the power generation of the two expanders and the work consumed by P1 and P2 remains unchanged.

(4). The cold water leaving LTA and the subcooled water from the P1 outlet converge at the HX1 inlet. Consequently, $m_1 = m_2 + m_3$.

(5). As the water in HTA is in the gas-liquid coexistence state consistently, its temperature and pressure are invariable. The same is true for LTA.

(6). m_2 is determined by the inlet condition of the flue gas and it can be adjusted by P3. At the nominal condition (i.e., the heat provided by the heat source equals the heat required by the RC-ORC), the mass flow of water from LTA to HTA (m_2) equals that from HTA to LTA (m_5). Owing to $m_2 = m_5$, equation $m_1 = m_5 + m_3$ holds. Both accumulators are in the state of mass conservation and their water level is maintained constant, respectively.

(7). m_2 rises when the inlet temperature or mass flow of the flue gas increases (or in other words, the heat delivered by the flue gas exceeds the nominal demand by the RC-ORC), which immediately leads to the increment of m_1. $m_2 > m_5$ and $m_1 > m_5 + m_3$ in this case. It indicates the mass flow of water leaving LTA (m_2) is larger than that of entering it (m_5). The weight of water in LTA decreases while it increases for HTA. The increased weight is equal to that reduced according to the law of conservation of mass. The water level of HTA rises while it falls for LTA. The excess heat from the heat source is stored in HTA and the system is in “Heat Storage” mode.

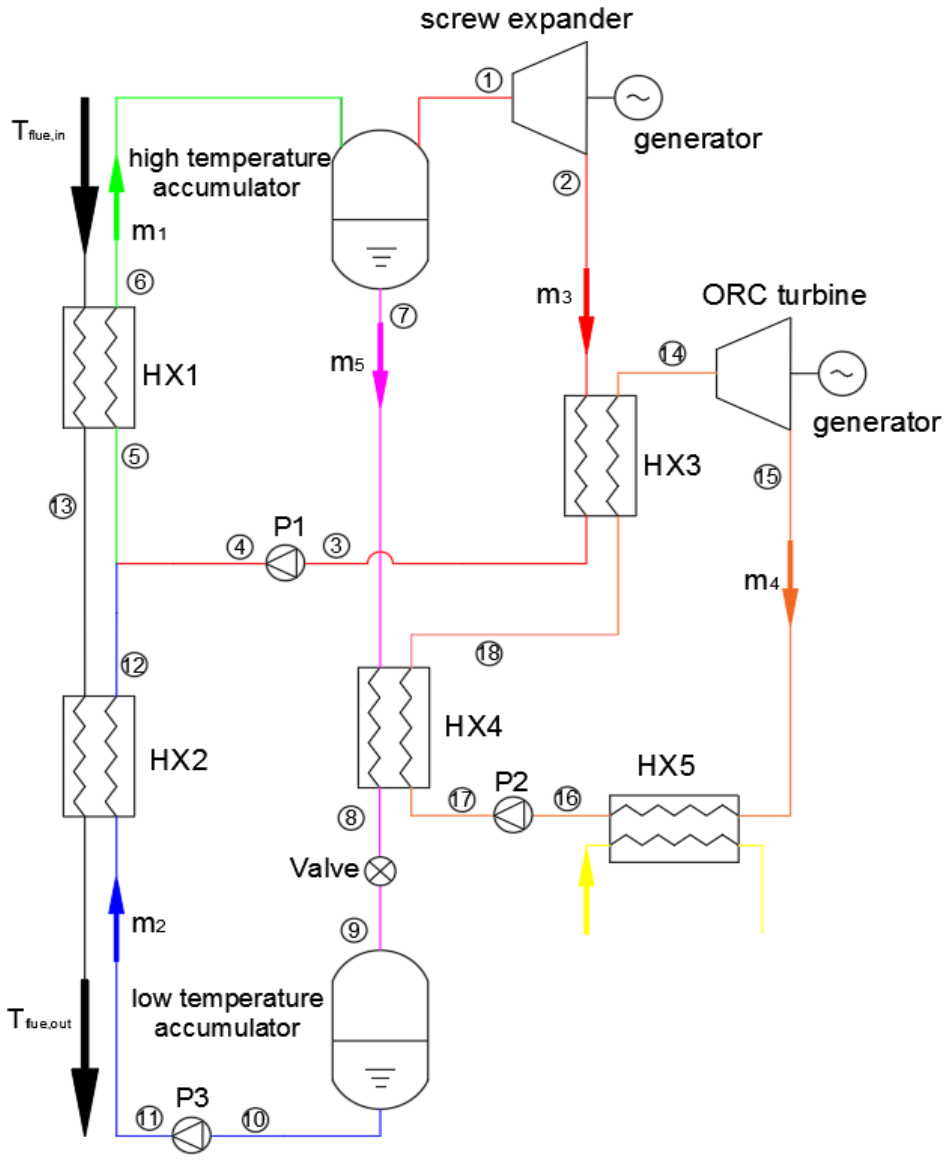

Fig. 2. Exhaust heat recovery system using RC-ORC and two-stage accumulators.

(8). Similar to (7), m_2 declines when the inlet temperature or mass flow of the flue gas is lower than that of the rated condition. m_1 reduces at this time and the water level of HTA drops. Correspondingly, the water level of LTA rises. The overall effect is that HTA continuously releases heat by mass transfer to maintain the normal operation of the RC-ORC. The system is in "Heat Discharge" mode at this time.

2.2 Features

The proposed system has the following features.

First, the introduction of two-stage steam accumulators into waste heat recovery is original. Existing dual-tank systems use thermal oil or molten salt as the storage medium, and they are only used to drive single-stage Rankine cycles [7]. Current steam storage is restricted to a single-tank method. Notably, the application of both dual-tank and steam options are limited to the solar thermal power plant at present [21, 22]. The integration of steam accumulators with waste heat recovery has not been reported yet.

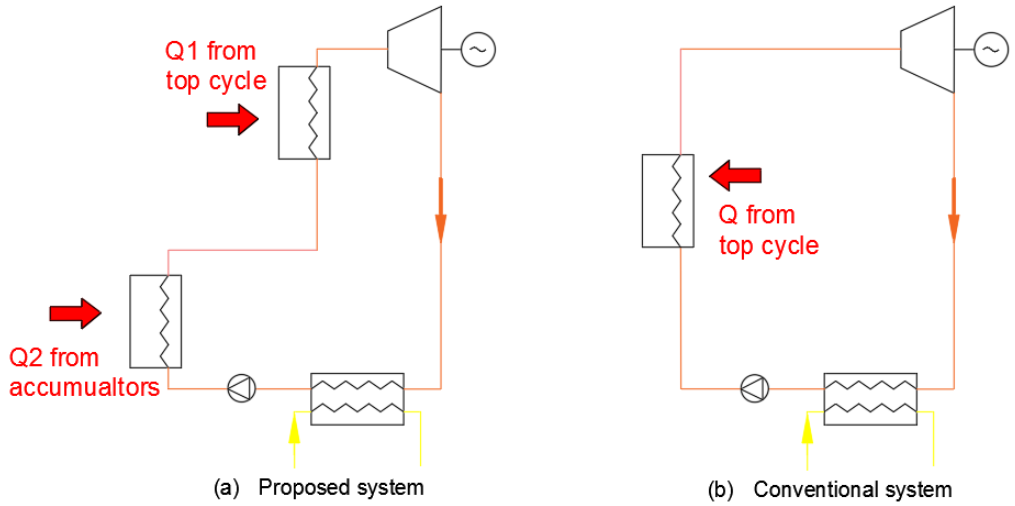

Fig. 3. The difference between the novel and conventional heating processes for ORC.

Second, the heating process of the ORC is unique. In a convectional RC-ORC system, the heat source of the ORC comes solely from the top RC [23-26]. By contrast, the ORC is driven parallelly by the top RC and accumulators in the proposed system as presented in Fig. 3. The mass flow rate from the HTA to LTA is constant and determined by the fluctuation of waste heat. The organic fluid in the ORC first absorbs the heat in the heat exchanger 4 (HX4) and partially vaporized, and then entirely vaporized after taking in heat from the condensation end of the top RC.

Third, both the heat storage and discharge modes are distinctive. The power conversion remains the same during charge and discharge. However, when the waste heat input is larger

than the nominal value, the mass flow rate of water through HX1 and HX2 is increased. The HTA is therefore charged with an increasing total mass. Similarly, heat is discharged from HTA with a decreasing mass as the waste heat input becomes lower than the rated condition.

2.3 Advantages

The foreseeable advantages can be elaborated into the following five aspects.

First, constant pressures in the accumulators can be maintained with relatively small volumes and lower cost. Conventional steam vessels produce steam by sliding pressure and flashing, the pressure of the supplied steam during discharge is lower than that of the nominal condition. Besides, temperature transients result in thermo-mechanical stress and sliding pressure causes plastic deformation. All these factors reduce the lifespan of the container. Furthermore, the temperature drop of water is small (generally＜50 °C) to avoid extremely inefficient power generation of the expander, thereby leading to a limited storage capacity. Nevertheless, flashing is omitted in the proposed system. When the heat source fluctuates, the heat received by the RC-ORC can be maintained constant purely through adjusting m_2. The temperature and pressure of both tanks remain unchanged, respectively, which is favorable for their operation. The supplied saturated steam is steady, and its temperature and pressure are the same as those of HTA invariably. More importantly, the required tank volume is much smaller than the Ruths vessels, which will be specified in Section 4.

Second, stable power conversion is guaranteed. In existing dual-tank arrangements as graphed in Fig. 4, the hot tank is connected with the cold tank via the steam generator, or through the thermal oil-molten salt HX. The heat storage and discharge processes are carried out separately in time. The discharge duration is determined by the storage capacity of tanks (generally＜10 h) and all the energy used to generate steam comes from the heat released

during the discharge process. By comparison, the heat release and storage are implemented simultaneously in the proposed system. The amount of stored heat varies depending on the heat source. The released heat remains constant since m_5 is perpetual, and it purely provides partial heat for the bottom ORC. The two expanders, P1 and P2 consistently work under the nominal condition, while the water level of the two accumulators waxes and wanes.

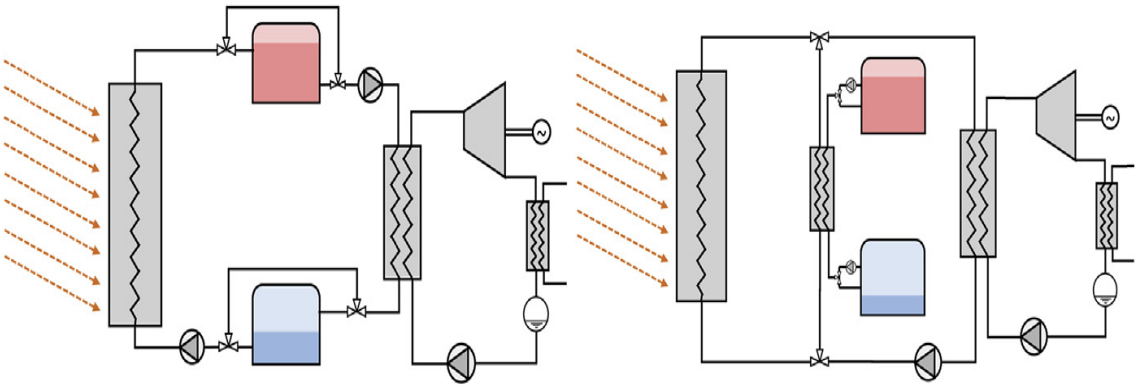

Fig. 4 Direct (left) and indirect (right) dual-tank thermal energy storage.

Third, the waste heat recovery rate is increased. Restricted by the heat transfer temperature difference, the evaporation temperature of the bottom cycle is lower than the condensation temperature of the top cycle in the conventional cascade Rankine cycles [24, 25]. Meanwhile, the temperature of the flue gas to be exhausted to the environment is higher than the condensation temperature of the top cycle, resulting in insufficient heat recovery. By contrast, the heat used to drive the top RC ($m_3(h_1 - h_4)$) is merely part of the energy released by the flue gas in Fig. 2. The flue gas will be further condensed after passing through HX2. It is possible to achieve a flue gas outlet temperature lower than the ORC evaporation temperature for the proposed system. The exergy contained in the exhaust heat can be extracted more adequately through this inimitable structural design.

Fourth, the system combines the advantages of stream control and latent heat storage options and overcomes some of their defects as well. The drawback of heat being wasted when the heat

source deviates from the design conditions in the stream control scheme is eliminated. Although steam is adopted as the medium, it has the same characteristic as the latent heat storage technique in which the medium temperature remains constant during charging and discharging. The concerns to the slow thermal response, recession of thermophysical properties and high cost of PCMs are dispelled.

Fifth, the grade of waste heat and thermodynamic cycle match automatically. Higher inlet temperature or mass flow of the flue gas leads to a poorer quality of steam entering HTA, which will be pointed out in Section 4. The grade of steam generated from HTA is high, which is especially suited to drive the RC-ORC. While the grade of water stored in HTA is low, which is suitable to preheat the bottom ORC fluid. This conforms to the optimization principle of energy cascade utilization.

3. Mathematical models

3.1. Thermodynamic models

3.1.1. Flue gas

In cement production, waste air that cools down the produced clinker is usually found in the range 150-350 °C [27]. After experiencing the initial instability, the temperature shows a wavelike undulation between 220 °C and 320 °C as recorded by Legmann et al. [7, 28]. The mass flow is considered close to 54 kg/s [29]. In steel production, a flue gas recuperator at the rolling mill furnace can ensure a constant temperature (approximately 400 °C), whereas the mass flow undergoes irregular fluctuations [7]. On these bases, two simplified cases are proposed, namely, Case Ⅰ (The mass flow of flue gas (m_{flue}) is kept at 50 kg/s and the inlet temperature ($T_{flue,in}$) is a sinusoidal function varying from 220 °C to 320 °C as depicted in Fig. 5 (a)) and Case Ⅱ ($T_{flue,in}$ is kept at 400 °C and m_{flue} is a zigzag function ranging from 18

kg/s to 12 kg/s as shown in Fig. 5(b)). The period of both functions is 1 h.

In addition, the following assumptions are made:

a. The main component of the flue gas is air and its enthalpy at different temperatures can be obtained from REFPROP 8.0 [30]. Pressure has little effect on the enthalpy of air according to the query results of REFPROP.

b. The exhaust gas is available 24 h/day and the operation duration of the system is 24 h/day.

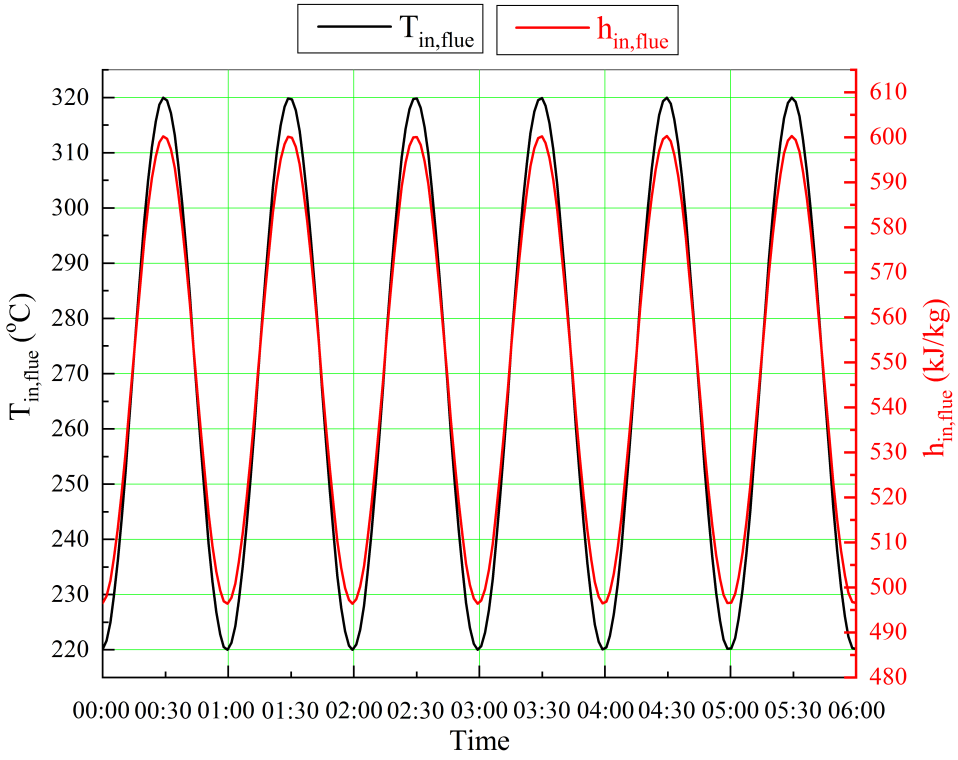

(a)

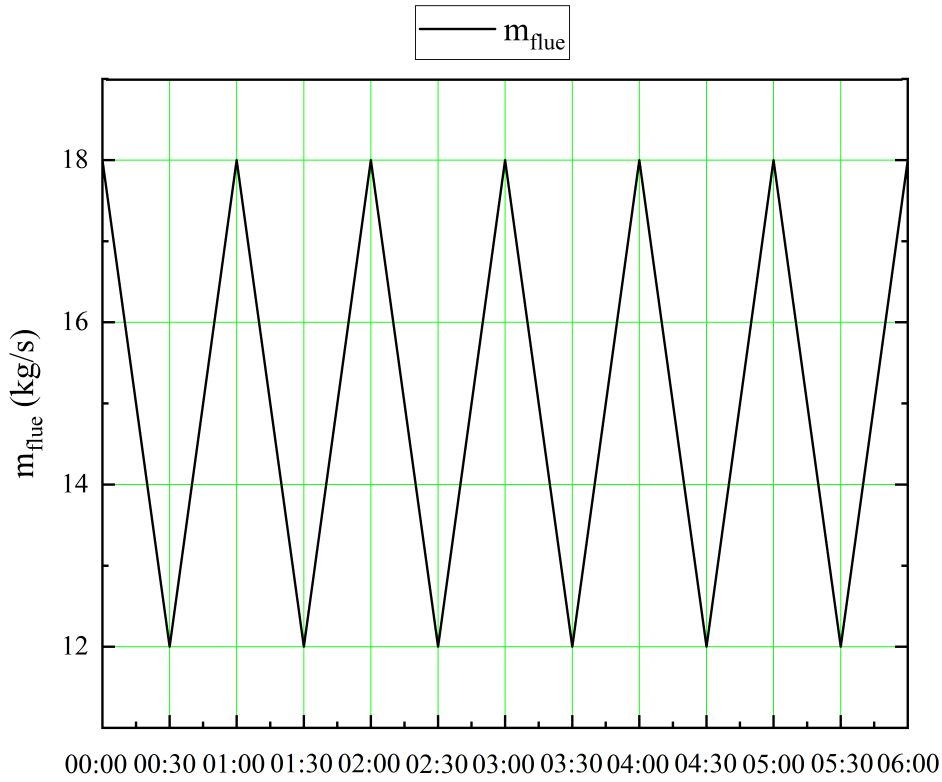

(b)

Fig. 5. Variations of flue gas (a) inlet temperature and enthalpy with time in Case Ⅰ and (b) mass flow rate with time in Case Ⅱ.

c. In order to prevent the corrosion of the heating surface caused by the acid vapor (composed of SO_2, SO_3, NO, NO_2, etc.), the final exhaust temperature ($T_{flue,out}$) should be higher than the acid dew point. $T_{flue,out}$ is fixed at 120 °C ($h_{flue,out}$ =394.35 kJ/kg) in this study.

$T_{flue,in}$ in Case Ⅰ is described by

$$T_{flue,in} = 50sin\,(2\pi\tau - \frac{\pi}{2}) + 270 \quad (1)$$

where τ is the hour at the corresponding moment and $\tau \in [0, 24]$.

Given $T_{flue,in}$ and the inlet pressure of 0.1 MPa, the inlet enthalpy of air ($h_{flue,in}$) can be obtained from REFPROP. $h_{flue,in}$ is also a sinusoidal function varying with time as exhibited in Fig. 5 (a). $h_{flue,in}$ can be approximately expressed by

$$h_{flue,in} = 51.95sin\,(2\pi\tau - \frac{\pi}{2}) + 548.35 \quad (2)$$

m_{flue} in Case Ⅱ is a piecewise function. The first period of m_{flue} is defined by

$$m_{flue} = \begin{cases} -16\tau + 18 & \tau \in [0, 0.5] \\ 16\tau + 2 & \tau \in [0.5, 1] \end{cases} \quad (3)$$

To maximize the average steam generation rate (m_3) and thus the power output, it is assumed that all the heat generated by the enthalpy drop of flue gas in the binary phase of HX1 is transferred to the top RC fluid and transforms it from saturated water to saturated steam. Simultaneously, the cold water from the outlet of P3 is merely heated to saturated water after flowing through HX2 and HX1. In other words, the heat released by the flue gas is divided into two parts: one part is used to supply the energy required for the heat-absorbing process of the top RC (heats the subcooled water at the outlet of P1 to dry saturated steam); the rest is transferred to the cold water at the outlet of P3 and turns it into saturated water. Assume that the evaporation temperature of water (T_6) is 200 °C. The energy conservation equation in HX1 and HX2 can be acquired based on the above analysis.

$$m_{flue}\left(h_{flue,in} - h_{flue,out}\right) = m_2(h_{sl} - h_{11}) + m_3(h_{ss} - h_4) \quad (4)$$

where h_{sl} and h_{ss} represent enthalpies of saturated liquid and saturated steam at 200 ºC, respectively (h_{sl} =852.27 kJ/kg, h_{ss} =2792 kJ/kg).

From another point of view, the mass flow of binary phase steam flowing into HTA can be deemed as the mixture of the saturated steam and saturated water (i.e., $m_1 = m_3 + m_2$). The conservation of energy equation is expressed by

$$m_1 h_6 = m_3 h_{ss} + m_2 h_{sl} \quad (5)$$

The mass flow of saturated steam entering and leaving HTA is the same (both are m_3).

Suppose the minimum heat transfer temperature difference (ΔT_{min}) is 10 °C. m_3 during a function period (1 h) can be calculated by

$$\int_0^1 3600 m_{flue}(h_{flue,in} - h_{flue,210℃})\, d\tau = 1 \times 3600 \times m_3(h_{ss} - h_{sl}) \quad (6)$$

where $h_{flue,210℃}$ denotes the enthalpy of flue gas corresponding to the saturated water at 200 °C. $h_{flue,210℃}$ =486.13 kJ/kg.

3.1.2. Accumulators

The mass of water in LTA returns to the initial value after a complete period of the function, i.e., the mass of water leaving LTA equals that of flowing into it in 1 h.

$$\int_0^1 3600 m_2\, d\tau = 1 \times 3600 m_5 \quad (7)$$

The water level in both accumulators fluctuates with $T_{flue,in}$. The variation of the water mass in HTA within arbitrary τ (Δm_{HTA}) can be written as the difference between the mass of the inlet water and that of the outlet water.

$$\Delta m_{HTA} = \int_0^\tau 3600 m_2\, d\tau - \int_0^\tau 3600 m_5\, d\tau \quad (8)$$

Since the mass flow of saturated steam entering and leaving HTA is the same, the saturated steam can be ignored in the volume design of HTA. The required minimum volume of water ($V_{water,min}$) is expressed by

$$V_{water,min} = \frac{\Delta m_{HTA,max}}{\rho_{water,200℃}} \quad (9)$$

3.1.3. Heat exchangers

As the temperature and pressure of HTA are maintained constant (200 °C and the corresponding saturation pressure of 1.56 MPa), the pressure of fluid entering HTA equals that leaving it. It can be inferred that $p_{11} = p_{12} = p_4 = p_5 = p_6 = p_1 = p_7 = p_8$ =1.56 MPa under the assumption that the pressure drop in HXs is ignored.

h_5 can be obtained from the energy conservation equation of the mixing process at the inlet of HX1.

$$m_1 h_5 = m_3 h_4 + m_2 h_{12} \quad (10)$$

The heat balance in HX1~HX4 is defined as

$$m_{flue}(h_{flue,in} - h_{13}) = m_1(h_6 - h_5) \tag{11}$$

$$m_{flue}(h_{13} - h_{flue,out}) = m_2(h_{12} - h_{11}) \tag{12}$$

$$m_3(h_2 - h_3) = m_4(h_{14} - h_{18}) \tag{13}$$

$$m_5(h_7 - h_8) = m_4(h_{18} - h_{17}) \tag{14}$$

3.1.4. Expanders

The work produced by the SE and ORC turbine is determined by

$$W_{SE} = m_3(h_1 - h_2) = m_3(h_1 - h_{2s})\varepsilon_{ST} \tag{15}$$

$$W_{OT} = m_4(h_{14} - h_{15}) = m_4(h_{14} - h_{15s})\varepsilon_{OT} \tag{16}$$

where ε_{ST} and ε_{OT} denote the isentropic efficiencies of SE and ORC turbine, respectively.

3.1.5. Pumps

The work consumed by P1 and P2 is calculated by

$$W_{P1} = m_3(h_4 - h_3) = m_3(h_{4s} - h_3)/\varepsilon_P \tag{17}$$

$$W_{P2} = m_4(h_{17} - h_{16}) = m_4(h_{17s} - h_{16})/\varepsilon_P \tag{18}$$

where ε_P is the pump isentropic efficiency.

In the "Heat Discharge" process, water flows from HTA to LTA and the heat serves as a partial heat source for the evaporation of ORC fluid. For further circulation, it is necessary to pump back the water into HTA to supplement the diminishing water. The required pump power is defined as

$$W_{P3} = m_2(h_{11} - h_{10}) = m_2(h_{11s} - h_{10})/\varepsilon_P \tag{19}$$

3.1.6. Net power output

The pressure after throttling equals the saturation pressure corresponding to the temperature before throttling. The enthalpy value after throttling is the same as that before throttling

$$h_9 = h_8 \tag{20}$$

The power loss caused by the valve is calculated by

$$W_{loss} = m_5(h_8 - h_{9s}) \tag{21}$$

The net generated power by the system is expressed by

$$W_{net} = (W_{SE} + W_{OT}) \cdot \varepsilon_g - W_{P1} - W_{P2} - W_{P3} \tag{22}$$

where ε_g is the generator efficiency.

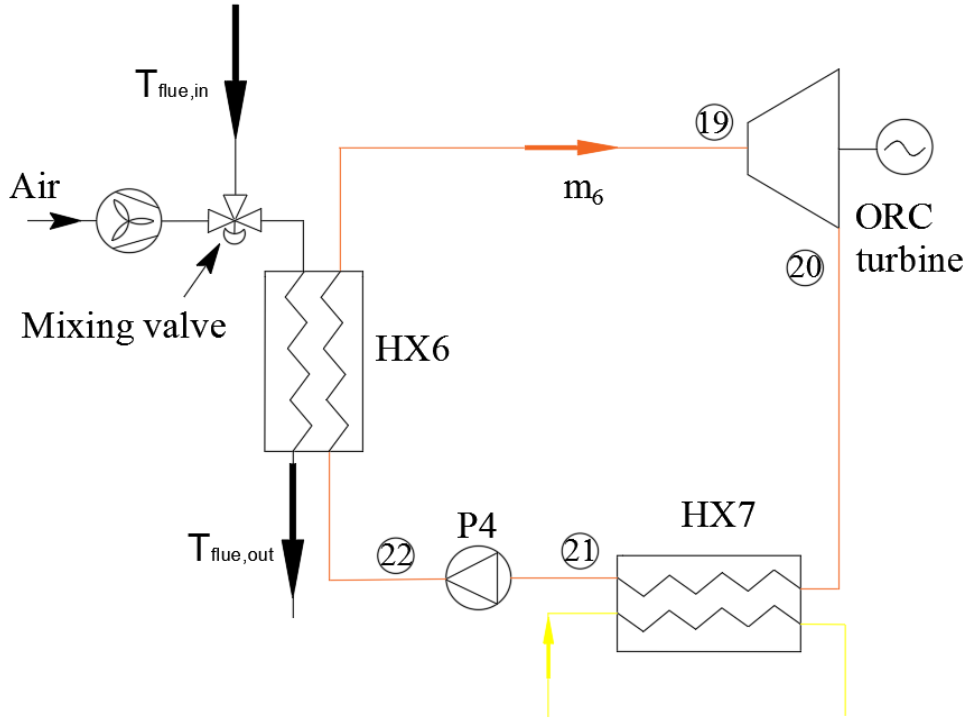

Fig. 6. Conventional single-stage ORC with stream control.

3.1.7. Thermal efficiency

The heat input to the RC-ORC includes two parts: the heat absorbed by the top RC ($m_3(h_1 - h_4)$) and that by ORC fluid in HX4 (i.e., the heat released from HTA to LTA, $m_5(h_7 - h_8)$). The thermal efficiency is defined by

$$\eta_t = \frac{W_{net}}{m_3(h_1 - h_4) + m_5(h_7 - h_8)} \tag{23}$$

To highlight the advantages of the novel system, a conventional single-stage ORC with

stream control is presented in Fig. 6 for comparison. Its thermal efficiency is

$$\eta_{t,ss} = \frac{m_6(h_{19}-h_{20})\cdot\varepsilon_g - m_6(h_{22}-h_{21})}{m_6(h_{19}-h_{22})} \tag{24}$$

3.2. Economic models

3.2.1. Accumulators

The design of accumulators refers to the Boiler and Pressure Vessel Code of the American Society of Mechanical Engineers (ASME) [31] and the details are presented in Appendix A.

3.2.2. Other units

The cost of large HXs is mainly contributed by the heat transfer area and hence the total amount of materials in use [32]. HTRI software is the industry's most advanced thermal process design and simulation software [33], and it is used to estimate the HX area. Details on the area calculation are provided in Appendix B. The cost estimating equations are presented in Appendix C.

3.2.3. Normalized investment cost

The normalized investment cost (NIC) for the cascade system is expressed by

$$NIC_{cascade} = \frac{C_{cascade}}{W_{net}} \tag{25}$$

where $C_{cascade}$ is the initial investment of the cascade system

$$C_{cascade} = \sum_{i=1}^{5} C_{BM,HXi} + \sum_{i=1}^{3} C_{BM,Pi} + C_{BM,turbine} + C_{p,SE} + C_{p,turbine,g} + C_{p,SE,g} + C_{HTA} + C_{LTA} \tag{26}$$

For the single-stage ORC,

$$NIC_{ss} = \frac{C_{ss}}{W_{net,ss}} \tag{27}$$

where C_{ss} is the total cost of the single-stage ORC

$$C_{ss} = C_{BM,HX6} + C_{BM,HX7} + C_{BM,P4} + C_{BM,turbine,ss} + C_{p,turbine,g,ss} \tag{28}$$

3.2.4. Equivalent payback period

Given the heat source, the cascade system may generate more electricity than the single-stage ORC. An equivalent payback period (EPP) is introduced as

$$EPP = \frac{C_{cascade} - C_{ss}}{Y_{cascade} - Y_{ss}} \tag{29}$$

$Y_{cascade}$ is the annual revenue of electricity

$$Y_{cascade} = 365 \cdot \int_0^{24} W_{net} \cdot d\tau \cdot C_{elec} \tag{30}$$

where the electricity price (C_{elec}) is 0.18 \$/kWh [34].

4. Results and discussion

Table 1. Specific parameters.

Term	Value
SE efficiency, $\boldsymbol{\varepsilon_{SE}}$	0.75
ORC turbine efficiency, $\boldsymbol{\varepsilon_{OT}}$	0.75
Generator efficiency, $\boldsymbol{\varepsilon_{g}}$	0.95
Pump efficiency, $\boldsymbol{\varepsilon_{P}}$	0.75
Minimum heat transfer temperature difference, $\boldsymbol{\Delta T_{min}}$	10 °C
Flue gas outlet temperature, $\boldsymbol{T_{flue,out}}$	120 °C
ORC condensation temperature, $\boldsymbol{T_{16}}$ and $\boldsymbol{T_{21}}$	35 °C
Steam evaporation temperature, $\boldsymbol{T_{1}}$	200 °C
ORC evaporation temperature, $\boldsymbol{T_{14}}$	120 °C
Welded joint efficiency, $\boldsymbol{E}$	0.8
Density of steel, $\boldsymbol{\rho_{steel}}$	7850 kg/m^3
Gravity, $\boldsymbol{g}$	9.8 N/kg
Additional thickness for corrosion allowance, $\boldsymbol{t_{CA}}$	3.175 mm

$CEPCI_{2001}/CEPCI_{2018}$	397/648.7
Electricity price, C_{elec}	0.18 $/kWh

Pentane is selected as the representative bottom ORC fluid because it is widely adopted by Ormat Technologies Inc. [35], which has built more than 1000 ORC plants of up to 1701 MW [36]. The assumptions are listed in Table 1.

4.1. Thermodynamic performance in Case Ⅰ.

Table 2. Parameters of the fixed state points.

State point	Temperature (°C)	Pressure (MPa)	Enthalpy (kJ/kg)	Dryness (%)
1	200	1.56	2792	100
2	130	0.27	2557.78	92.53
3	130	0.27	546.38	0
4	130.22	1.56	548.19	subcooled
6	200	1.56	varied	varied
7	200	1.56	852.27	0
8	45.47	1.56	191.75	subcooled
9	45.47	0.01	191.75	0.06
10	45.47	0.01	190.40	0
11	45.65	1.56	192.48	subcooled
14	120	0.91	490.59	100
15	73.95	0.10	427.25	superheated
16	35	0.10	-2.52	0

17	35.47	0.91	-0.75	subcooled
18	120 (80.53)	0.91	274.38 (110.94)	20.26 (subcooled)

Except for 5, 12 and 13, all other fixed state points can be obtained according to Section 3 and they are posted in Table 2. The thermodynamic state of point 18 differs in the two cases, and the results for Case Ⅱ are shown in the brackets. It can be calculated that m_3 =1.604 kg/s from Eq. (5). m_2 can be evaluated by combining Eqs. (2) and (4).

$$m_2 = 3.937 sin\left(2\pi\tau - \frac{\pi}{2}\right) + 6.216 \tag{31}$$

m_1 can be determined by the mass conservation: $m_1 = m_2 + m_3 = 3.937 sin\left(2\pi\tau - \frac{\pi}{2}\right) + 7.82$. m_5 of 6.216 kg/s can be calculated by combining Eqs. (7) and (31). It can be obtained m_4 =14.923 kg/s and h_{18} =274.38 kJ/kg by solving Eqs. (13) and (14). As $m_2 = m_5$ under the rated condition, $sin\left(2\pi\tau - \frac{\pi}{2}\right) = 0$ and $T_{flue,in}$ = 270 °C can be easily deduced by comparing Eqs. (31) and (1). The rated condition corresponds to 00:15, 00:45, 01:15, 01:45⋯05:45. According to Eq. (31), $m_{2,\max}$ =10.153 kg/s when $T_{flue,in}$ =320 °C and $m_{2,\min}$ =2.279 kg/s when $T_{flue,in}$ =220 °C. m_2 =6.216 kg/s at the rated condition of $T_{flue,in}$ =270 °C.

Notably, the parameters of points 5, 12 and 13 change with the variation of $T_{flue,in}$ or m_{flue}. Even $T_{flue,in}$ or m_{flue} is given, there are many possible values for the three points. They are closely related to the design area of HX1 and HX2, thus affecting the economy of the system. Given an arbitrary moment, h_6 and x_6 can be determined according to Eqs. (5) and (31). h_6 =1653.54 kJ/kg and x_6 =41.31% when $T_{flue,in}$ =220 °C. h_6 =1250.14 kJ/kg and x_6 =20.51% at the rated condition, while they drop to 1116.91 kJ/kg and 13.64% when $T_{flue,in}$ climbs to 320 °C. Consequently, both h_6 and x_6 decrease as $T_{flue,in}$ elevates.

Table 3. The work output or consumed in Case Ⅰ.

Work	W_{P1}	W_{P2}	W_{P3}	W_{loss}	W_{SE}	W_{OT}	W_{net}
kW	2.90	26.41	4.74-21.12	9.70	375.69	945.22	1204.43-1220.81

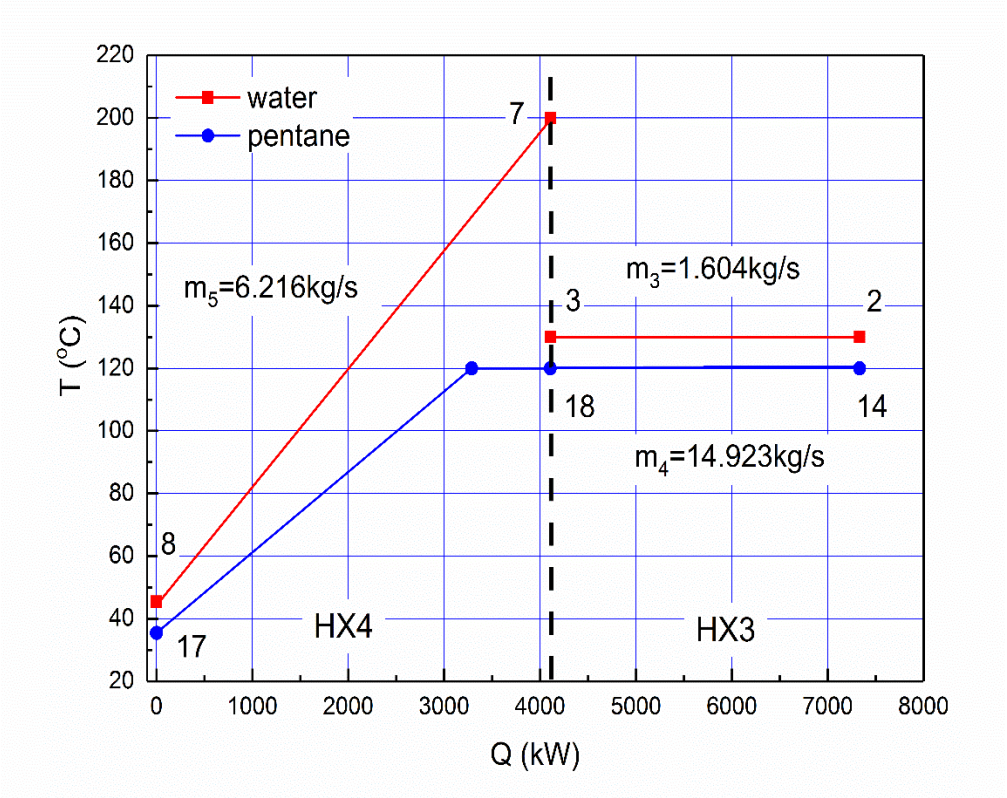

Fig. 7. *T-Q* diagram in HX4 and HX3.

The work output or consumed by each component is provided in Table 3. The electricity output by ORC turbine is roughly 2.5 times that of SE. W_{net} fluctuates by 16.38 kW due to the variation of W_{P3}. η_t ranges from 15.63% to 15.84%.

The *T-Q* diagram in HX4 and HX3 is presented in Fig. 7. The whole graph is divided into two parts by the dotted line. The left half signifies HX4 and the right half stands for HX3. The transferred heat is 4105.79 kW for HX4 and 3226.29 kW for HX3. ΔT_{min} takes place at the pentane inlet for HX4, while it is maintained at 10 °C for HX3.

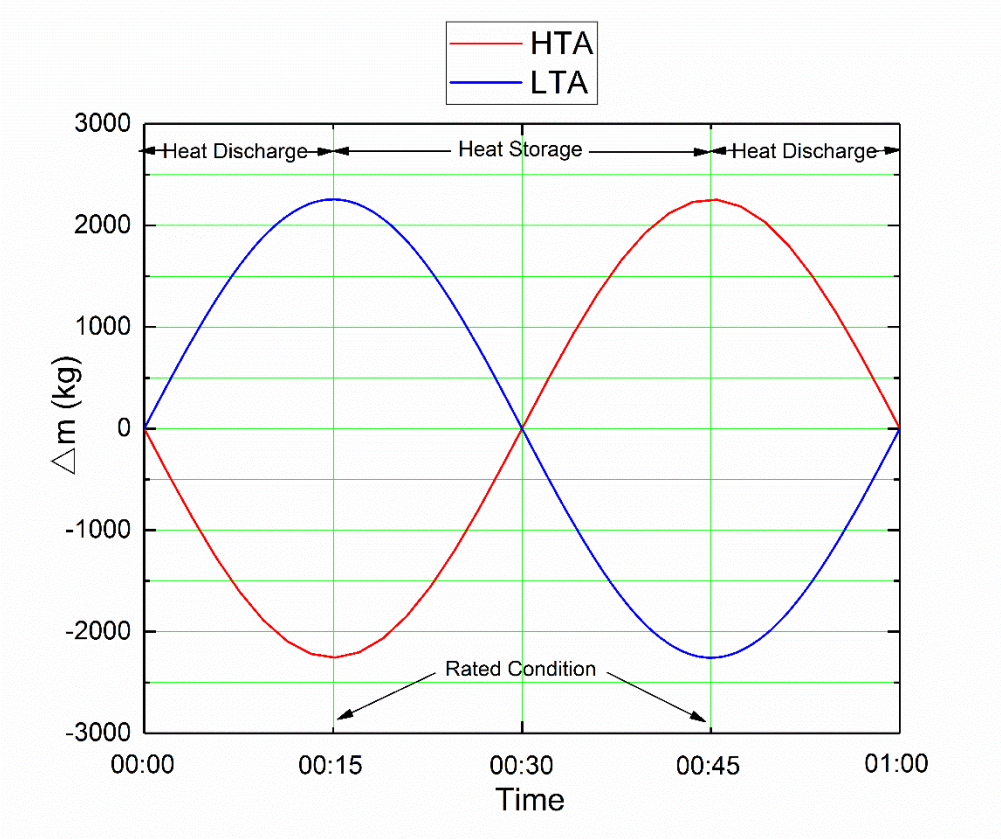

Fig. 8. Variations of Δm in the two accumulators in the first period of Case Ⅰ.

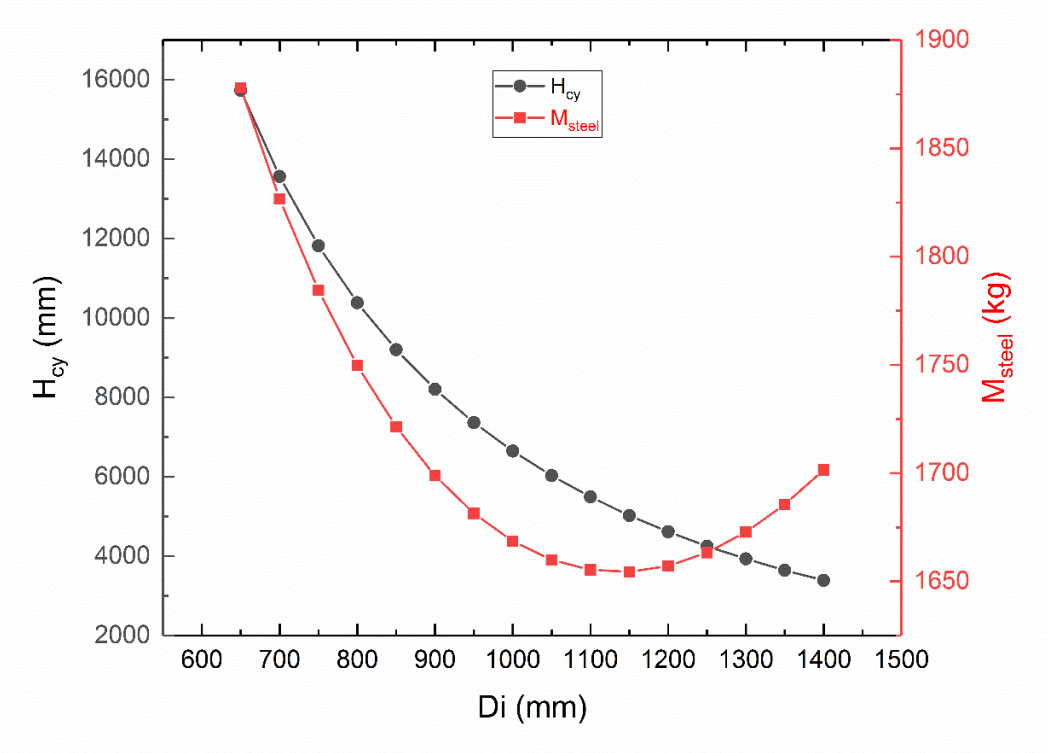

Fig. 9. Variations of H_{cy} and M_{steel} with D_i for HTA.

Δm_{HTA} can be drawn by simplifying Eq. (8)

$$\Delta m_{HTA} = -2255.73cos\left(2\pi\tau - \frac{\pi}{2}\right) \quad (32)$$

$\Delta m_{LTA} = -\Delta m_{HTA} = 2255.73cos\left(2\pi\tau - \frac{\pi}{2}\right)$.Variations of Δm in the two accumulators in the first period are depicted in Fig. 8. The periods from 00:00 to 00:15 and from 00:45 to 01:00 are the "Heat Discharge" mode. The "Heat Storage" mode lasts from 00:15 to 00:45. Δm_{HTA} reaches the minimum (-2255.73 kg) and the maximum (2255.73 kg) at the rated moments of 00:15 and 00:45, respectively. $\rho_{water,200°C}$ of 864.66 kg/m^3 can be acquired from REFPROP and $V_{HTA,min}$ =5.22 m^3 according to Eqs. (9) and (37). Similarly, $V_{LTA,min}$ =4.56 m^3 in view of $\rho_{water,45.47°C}$ =989.98 kg/m^3.

Table 4. Design parameters of HTA and LTA in Case Ⅰ.

Parameters \ Accumulator	HTA	LTA
$\boldsymbol{D_i}$ (mm)	1150	1150
$\boldsymbol{p}$ (MPa)	1.56	0.01
$\boldsymbol{H_{cy}}$ (mm)	5026	4390
$\boldsymbol{\delta_{cy}}$ (mm)	10.387	4.763
$\boldsymbol{V_{stell,cy}}$ (m^3)	0.19	0.076
$\boldsymbol{\delta_{head}}$ (mm)	7.167	4.763
$\boldsymbol{M_{stell,head}}$ (kg)	80.35	53.40
$\boldsymbol{M_{stell,cy}}$ (kg)	1493.8	595.5
$\boldsymbol{M_{stell}}$ (kg)	1654.5	702.3
$\boldsymbol{C_{stell}}$ ($)	917	389

Variations of H_{cy} and M_{steel} with D_i for HTA are illustrated in Fig. 9. M_{steel} first decreases and then increases with the enlarged D_i. $M_{steel,min}$ of 1654.5 kg is achieved at D_i of 1150 mm. As the internal pressure is 0.0098 MPa for LTA, general vacuum vessels can meet

the pressure requirements and the minimum design cylinder thickness of 4.763 mm (set by the ASME code [37]) is adopted. Design parameters of the two accumulators are indexed in Table 4. The steel cost of HTA is more than twice that of LTA. The total price of steel is 1306 $. Taking into account the budgets for design, processing, transportation and auxiliary materials, the overall cost of storage is expected to be less than 3000 $.

4.2. Thermodynamic performance in Case Ⅱ.

$h_{flue,in}$ remains 685.04 kJ/kg due to the fixed $T_{flue,in}$ of 400 °C. Analogous with Case Ⅰ, it can be deduced that m_3 =1.538 kg/s, m_5 =1.378 kg/s, m_4 =8.149 kg/s and the first period of m_2 is

$$m_2 = \begin{cases} -5.287\tau + 2.7 & \tau \in [0,0.5] \\ 5.287\tau - 2.587 & \tau \in [0.5, 1] \end{cases} \tag{33}$$

m_2 is also a piecewise linear function. The rated condition corresponds to 00:15, 00:45, 01:15, 01:45⋯05:45. $m_{2,\max}$ =2.7 kg/s when m_{flue} =18 kg/s and $m_{2,\min}$ =0.057 kg/s when m_{flue} =12 kg/s. m_2 =1.379 kg/s at the rated condition of m_{flue} =15 kg/s. Both h_6 and x_6 increase as m_{flue} reduces. For instance, h_6 = 1556.21 kJ/kg and x_6 = 36.29% when m_{flue} =18 kg/s. h_6 =1875.35 kJ/kg and x_6 =52.74% at the rated condition, while they rise to 2722.68 kJ/kg and 96.43% when m_{flue} = 12 kg/s. The work output or consumed is displayed in Table 5. There is a fluctuation of 5.5 kW in W_{net} and η_t ranges from 19.57% to 19.70%. The transferred heat is 910.20 kW for HX4 and 3093.53 kW for HX3.

Table 5. Results of the work output or consumed in Case Ⅱ.

Work	W_{P1}	W_{P2}	W_{P3}	W_{loss}	W_{SE}	W_{OT}	W_{net}
kW	2.78	14.42	0.12~5.62	2.15	360.23	516.16	853.57-859.06

Table 6. Design parameters of HTA and LTA in Case Ⅱ.

Parameters \ Accumulator	HTA	LTA
$\boldsymbol{D_i}$ (mm)	800	800
$\boldsymbol{p}$ (MPa)	1.56	0.01
$\boldsymbol{H_{cy}}$ (mm)	2745	2387
$\boldsymbol{\delta_{cy}}$ (mm)	8.192	4.763
$\boldsymbol{V_{stell,cy}}$ (m^3)	0.057	0.029
$\boldsymbol{\delta_{head}}$ (mm)	4.986	4.763
$\boldsymbol{M_{stell,head}}$ (kg)	27.05	25.84
$\boldsymbol{M_{stell,cy}}$ (kg)	448.26	225.67
$\boldsymbol{M_{stell}}$ (kg)	502.36	277.36
$\boldsymbol{C_{stell}}$ ($)	278	154

Δm_{HTA} can be drawn by simplifying Eq. (8)

$$\Delta m_{HTA} = \begin{cases} -9516.6\tau^2 + 4759.2\tau & \tau \in [0, 0.5] \\ 9516.6\tau^2 - 14274\tau + 4758.3 & \tau \in [0.5, 1] \end{cases} \quad (34)$$

$\Delta m_{LTA} = -\Delta m_{HTA} = \begin{cases} -9516.6\tau^2 + 4759.2\tau & \tau \in [0, 0.5] \\ 9516.6\tau^2 - 14274\tau + 4758.3 & \tau \in [0.5, 1] \end{cases}$. Δm_{HTA} reaches the maximum (595.01 kg) and the minimum (-595.01 kg) at the rated moments of 00:15 and 00:45, respectively. $V_{HTA,min} = 1.38$ m^3 and $V_{LTA,min} = 1.20$ m^3. Design parameters of the two accumulators are reported in Table 6. The total price of steel is 432 $ and the overall budget for storage is probably within 1000 $.

Remarkably, flashing is not considered in this work due to the moderate fluctuations of the flue gas in both cases. When subjected to dramatic fluctuations in $T_{flue,in}$ or m_{flue}, transient flashing may occur. Nevertheless, it can be predicted that the duration and amplitude of the part-load operation are significantly lower than those of Ruths storage. Another effective method is to optimize the design parameters of the RC-ORC. The off-design operation can also

be omitted by setting lower inlet parameters of the expanders and thus smaller total power capacity.

4.3 Thermo-economic comparison with single-stage ORC

Case Ⅰ is exemplified. The physical parameters of flue gas can be attained by importing nitrogen and oxygen respectively from REFPROP according to their mass fraction in the air. S-type floating head HX is adopted on account of its competence in handling large temperature drop (＞50 °C), wide application, easy cleaning and maintenance. The fluid with higher pressure is located on the tube side to reduce the HX fabricating cost. Rod baffle is utilized to reduce the vibration and the flow resistance of the shell side fluid. As the flue gas is air with low heat transfer coefficient, the heat transfer coefficient of the shell side will be considerably low when the flue gas flows through HX1, HX2 and HX6. The same is true for the subcooled pentane in the shell side of HX4. The total heat transfer coefficient is not significantly improved and the required area will be large even if multiple (double or four-tube passes) tube passes are used because the overall heat transfer coefficient of an HX is lower than its weaker side. By contrast, only counterflow exists in the single-tube pass, which leads to the maximum logarithmic average heat transfer temperature difference and the minimum area. Accordingly, single-tube pass is employed in HX1, HX2, HX6 and HX4 while double-tube passes for the rest HXs. The cooling water rises from 20 °C to 25 °C in HX5 and HX7. The tube outer diameter of 19 mm and tube pitch of 25 mm are employed, which are common in industrial production. Over design area above 10% is ensured and the flow chart is exhibited in Fig. 10.

The inlet and outlet parameters of HX3~HX5 are determined, but the state points of 5, 12 and 13 vary with $T_{flue,in}$. The area of HX1 and HX2 should meet the maximum heat duty,

which corresponds to the most unfavorable condition of $T_{flue,in}$ =320 °C. h_{12}, h_5 and h_6 can be calculated from Eqs. (12), (10) and (11) respectively on the condition that T_{13} is defined. T_{13} ranges from 120 °C to 320 °C and there is an optimal T_{13} that minimizes the sum costs of HX1 and HX2. The optimization process is not carried out and the intermediate temperature of 220 °C is selected. It can be derived that h_{12} =695.04 kJ/kg, h_5 =675 kJ/kg and h_6 =1116.86 kJ/kg. The process data for HX1~HX5 is indexed in Table 7.

For the convenience of comparison, pentane is also adopted in Fig 6. The flue gas energy above 220 °C is wasted by mixing the inlet flue gas with cooling air. Similar to Fig. 1 (c), a steady heat source is maintained and the single-stage ORC works at stable conditions all along. Given ε_{OT}, ε_P and T_{21}, $W_{net,ss}$ varies with T_{19}. It can be calculated that the maximum $W_{net,ss}$ = 781.22 kW ($W_{OT,ss}$ = 888.00 kW, W_{P4} = 62.38 kW, m_6 = 9.240 kg/s and $\eta_{t,ss}$ =15.31%) by simple thermodynamic deduction. The optimized parameters are displayed in Table 8 and they are adopted for economic estimation. The process data for HX6 and HX7 is provided in Table 9.

Table 7. Parameters of HX1~HX5.

Process data	HX1	HX2	HX3	HX4	HX5
Shell side heat transfer coefficient, kW/m^2·K	0.200	0.241	16.445	0.403	1.154
Shell ID, mm	1900	1900	1000	1200	1100
Shell side velocity, m/s	42.16	40.42	0.87	0.04	5.89
Tube side heat transfer coefficient, kW/m^2·K	1.254	0.526	2.080	0.445	9.949
Tube length, m	3	3	6	10	9
Tube side velocity, m/s	0.03	0.02	4.28	0.02	2.63
Tube count	2988	3796	1045	1603	1316
Overall heat transfer coefficient, kW/m^2·K	0.157	0.145	0.984	0.176	0.747
Heat duty, MW	5.208	5.115	3.223	4.107	6.394
Inlet/Outlet height under nozzles, mm	400	200	0	0	0
Baffle central spacing, mm	200	100	300	100	200
Mean temperature difference, °C	73.9	64.4	9.8	27.5	13.7
Area, m^2	500.07	637.18	369.03	945.48	699.66
Over design, %	11.61	15.94	10.28	11.53	12.09

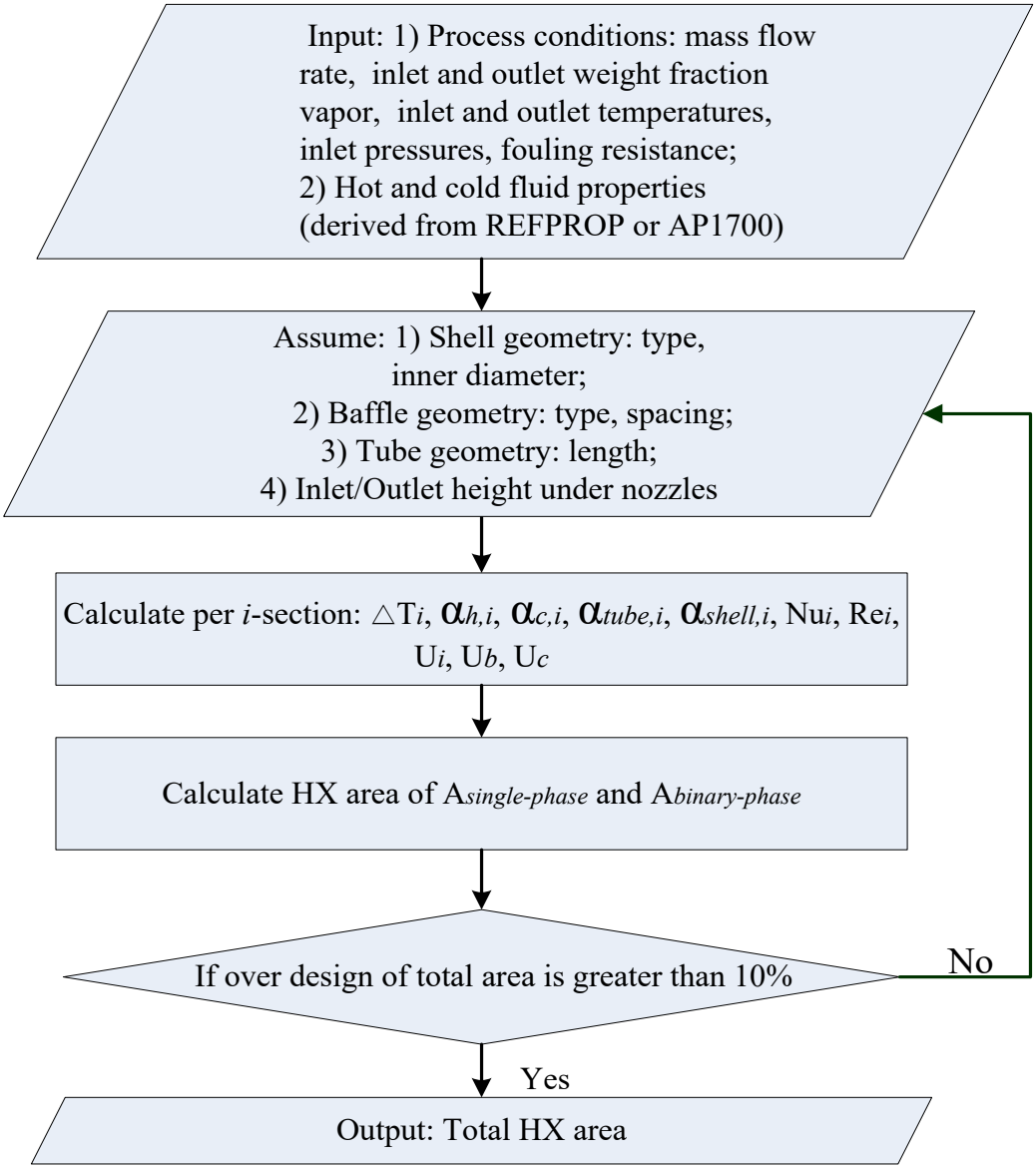

Fig. 10. Flow chart of the HX area calculation.

The cost for each unit is listed in Table 10. The investment in HXs accounts for roughly 50% in both systems respectively. The costs of the two turbines are comparable owing to their comparable power output. It can be obtained that C_{ss} =2.975 million \$ and NIC_{ss} =3808 \$/kW, $C_{cascade}$ =3.710 million \$ and $NIC_{cascade}$ =2883-2920 \$/kW, Y_{ss} =1.232 million \$, $Y_{cascade}$ =1.912 million \$ and EPP =1.08 years. Notably, the parameters in Table 2 are not thermodynamically optimized and EPP is expected to be shorter after optimization.

Table 8. Design parameters for single-stage ORC system.

State point	Temperature (°C)	Pressure (MPa)	Enthalpy (kJ/kg)	Dryness (%)
19	193	3.19	556.46	100
20	90.99	0.10	460.36	Superheated
21	35	0.10	-2.52	0
22	36.80	3.19	4.23	subcooled

Table 9. Parameters of HX6 and HX7.

Process data	HX6	HX7
Shell side heat transfer coefficient, kW/m^2·K	0.212	1.092
Shell ID, mm	2000	1000
Shell side velocity, m/s	40.37	4.79
Tube side heat transfer coefficient, kW/m^2·K	0.183	9.197
Tube length, m	10	8
Tube side velocity, m/s	0.03	2.38
Tube count	4625	970
Overall heat transfer coefficient, kW/m^2·K	0.083	0.715
Heat duty, MW	5.115	4.296
Inlet/Outlet height under nozzles, mm	0	100
Baffle central spacing, mm	150	150
Mean temperature difference, °C	25.7	14.5
Area, m^2	2681.04	458.31
Over design, %	12.14	10.49

Table 10. Cost for each unit (thousand $).

Cascade system	HX1	HX2	HX3	HX4	HX5	Turbine	Turbine generator
	329.92	381.20	273.06	491.01	415.60	1450.68	38.35
	SE	SE generator	P1	P2	P3	Accumulators	
	218.95	15.96	20.07	37.83	34.02	3.00	
Single-stage ORC system	HX6	HX7	Turbine	Turbine generator	P4		
	1117.74	322.88	1415.97	36.14	82.02		

5. Conclusion

A novel RC-ORC system combined with two-stage steam accumulators is innovatively introduced into the flue gas recovery. It has great potential to solve the problem of heat source fluctuations merely through the mass flow regulation of the water pump. The water level of the two tanks waxes and wanes, while constant temperature and pressure are maintained for them, respectively. The heat obtained by the RC-ORC remains the same and the system operates in the rated condition consistently.

The instabilities of temperature and pressure due to flashing in the Ruths storage are obviated through the unique operation modes of “Heat Storage” and “Heat Discharge” at constant temperature and pressure. The distinct connection between HTA and LTA makes the heat release process afford only partial energy for the bottom ORC. Simultaneously, the waste heat passes through the two-stage HX configuration to provide all the heat for the top RC and the water at the LTA outlet. The distinctive operational principle greatly reduces the irreversible loss of the heat source. Moreover, the system combines the advantages of conventional stream control and latent heat storage options and overcomes some of their shortcomings.

Two typical cases are analyzed: m_{flue} is stable and $T_{flue,in}$ presents a sinusoidal function

(Case Ⅰ); $T_{flue,in}$ is fixed and m_{flue} exhibits a zigzag function (Case Ⅱ). The variations in thermal efficiencies and power generation are slight (15.63-15.84% and 1204.43-1220.81 kW in Case Ⅰ, 19.57-19.70% and 853.57-859.06 kW in Case Ⅱ). The required volumes of the tanks are significantly reduced (less than 5.5 m^3 and 1.5 m^3 for Cases Ⅰ and Ⅱ, respectively) compared with the water tanks in the traditional flashing technology. The overall cost of steel is approximately 1306 $ for Case Ⅰ and 432 $ for Case Ⅱ. Although the initial investment on the novel RC-ORC system is larger, NIC is decreased by 888-925 $/kW compared with the stream control-based single-stage ORC. Besides, 0.68 million $ more annual profit of electricity can be generated and EPP is purely 1.08 years on the condition of Case Ⅰ.

Acknowledgment

This study was sponsored by the Anhui Provincial Natural Science Foundation (2008085QE235, 2008085QE224), Fundamental Research Funds for the Central Universities of China (JZ2020HGTA0074, JZ2020HGTA0047), DONGFANG ELECTRIC Dongfang Boiler Group CO., LTD. and China Postdoctoral Science Foundation (2019M662140).

Appendix A. Design of the accumulator

The material cost of the accumulator is

$$C_{steel} = P_{steel}M_{steel} = P_{steel}\rho_{steel}V_{steel} \times 10^{-9} \tag{35}$$

where C_{steel} is the steel cost. P_{steel} is the cost per kilogram. Cylinder vessel is adopted and the total volume of steel (V_{steel}) is a function of the internal diameter (D_i), thickness (t) and

height (H) of the vessel.

The cylinder thickness (t_{cy}) to withstand an internal pressure (p in gauge pressure) in a vessel of D_i is

$$t_{cy} = \frac{p \cdot D_i}{2S \cdot E - 1.2p} + t_{CA} \tag{36}$$

where the units of p and D_i are MPa and mm; S is the maximum allowable tensile stress; Low-alloy steel SA202-B is exemplified and the price is 3600 RMB/ton [38] (554 $/ton under the assumption that the exchange rate of RMB against the dollar is 0.154). As S(-29 °C)= S(343 °C) =146.1 MPa [37], S(200 °C)= S(45.47 °C) =146.1 MPa can be obtained by interpolating. E is a welded joint efficiency and ranges from 1.0 to 0.6. t_{CA} is an additional thickness for a corrosion allowance (3.175-6.35 mm).

The maximum permissible liquid inventory in the tank in the case of level shutoff is half the volume of the tank considering safety rules. The minimum volume of HTA ($V_{HTA,min}$) is expressed by

$$V_{HTA,min} = V_{water,min}/0.5 = \pi \cdot 0.25{D_i}^2 \cdot H_{cy} \cdot 10^{-9}/0.5 \tag{37}$$

The material mass used for the cylinder is

$$M_{steel,cy} = \pi t_{cy}\left(D_i + t_{cy}\right)H_{cy}\rho_{steel} \cdot 10^{-9} \tag{38}$$

Cylinder vessel generally has two elliptical heads at the top and the bottom as graphed in Fig. 11. The design thickness of head (t_{head}) is expressed by

$$t_{head} = \frac{pD_iK}{2S \cdot E - 0.2p} + t_{CA} \tag{39}$$

K is a geometric factor given by

$$K = \frac{1}{6}\left[2 + \left(\frac{D_i}{2h}\right)\right] \tag{40}$$

$K = 1$ for the case when $h = D_i/4$ (a 2:1 elliptical head).

The approximate formula for a 2:1 elliptical head is

$$M_{steel,head} = \frac{\pi}{4} {D_i}^2 \left[1 + \left(\frac{2h}{D_i}\right)^2 \left(2 - \frac{2h}{D_i}\right)\right] t_{head} \rho_{steel} \cdot 10^{-9} \quad (41)$$

The total mass of material used for the vessel is

$$M_{steel} = M_{steel,cy} + 2M_{steel,head} \quad (42)$$

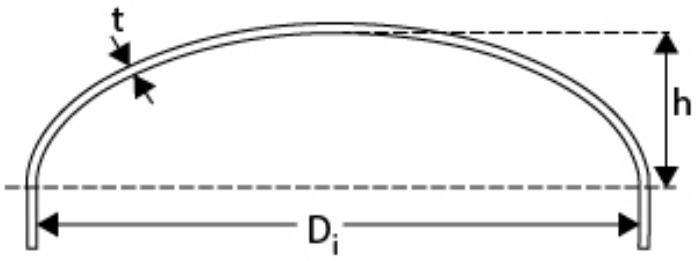

Fig. 11. Cross-section of the elliptical head.

Appendix B. HX area calculation

The heat transfer process is discretized into many subsections in which the thermodynamic properties of the working fluid are assumed to be constant.

1. Single-phase heat transfer

The required area in the ith subsection is expressed as

$$A_i = \frac{Q_i}{U_i \Delta T_i} \quad (43)$$

where Q is the heat duty in the ith subsection; U the overall heat transfer coefficient; ΔT is the log-mean temperature difference.

U_i is calculated as

$$\frac{1}{U_i} = \frac{1}{\alpha_{h,i}} + \frac{\delta}{\lambda} + \frac{1}{\alpha_{c,i}} \quad (44)$$

where α is the convection heat transfer coefficient of the fluid and subscript h and c represent the hot and cool fluid, respectively; δ and λ are the thickness and the thermal conductivity of the tube wall. δ is 2 mm in this work.

ΔT_i can be written as

$$\Delta T_i = \frac{(T_{h,i+1}-T_{c,i+1})-(T_{h,i}-T_{c,i})}{\ln\left(\frac{(T_{h,i+1}-T_{c,i+1}}{T_{h,i}-T_{c,i}}\right)} \tag{45}$$

The convection heat transfer coefficient of the tube side is given by the Petuk-hov correlation [39]

$$\alpha_{tube,i} = \frac{\lambda}{D_i}\left(\frac{\frac{f}{8}\cdot Re\cdot Pr}{12.7\left(\frac{f}{8}\right)^{0.5}\left(Pr^{\frac{2}{3}}-1\right)+1.07}\right) \tag{46}$$

where f is the Darcy resistance coefficient, and it is calculated by

$$f = \frac{1}{(1.82lgRe-1.64)^2} \tag{47}$$

The equation of the Reynolds number is:

$$Re_i = \frac{u_{tube,i}\cdot D_i}{\upsilon} \tag{48}$$

where $u_{tube,i}$ is the tubeside velocity, being expressed as:

$$u_{tube,i} = \frac{\dot{m}}{\rho_i\cdot N\cdot\pi\cdot\frac{D_i{}^2}{4}} \tag{49}$$

where N is the number of the tubes.

The equation of the Prandtl number is:

$$Pr = \frac{c_p\cdot\rho_i\cdot\upsilon}{\lambda} \tag{50}$$

The convection heat transfer coefficient for the shell side is [40]:

$$\alpha_{shell,i} = 0.36\left(\frac{\lambda}{D_{shell}}\right)\left(\frac{D_{shell}\cdot u_{shell}}{\upsilon}\right)^{0.55}\cdot Pr^{\frac{1}{3}}\left(\frac{\upsilon}{\upsilon_{tube}}\right)^{0.14} \tag{51}$$

2. Binary-phase heat transfer

For the evaporation process, the coefficient in the binary-phase region developed by Gungor and Winterton is used [41]

$$U_b = 0.023\left[\frac{G(1-\chi)d}{\rho\cdot\upsilon}\right]^{0.8} Pr^{0.4}\frac{\lambda}{d}\left[1+3000Bo^{0.86}+1.12\left(\frac{\chi}{1-\chi}\right)^{0.75}\left(\frac{\rho_l}{\rho_v}\right)^{0.41}\right] \tag{52}$$

where Bo is the boiling number:

$$Bo = \frac{q}{G \cdot (h_{ss} - h_{sl})} \tag{53}$$

For the condensation process, the coefficient in the binary-phase region is given by Shah [42]

$$U_c = 0.023 \left[\frac{G(1-\chi)d}{\rho \cdot \upsilon}\right]^{0.8} Pr^{0.4} \frac{\lambda}{d} \left[(1-\chi)^{0.8} + \frac{3.8\chi^{0.76}(1-\chi)^{0.04}}{Pr^{0.38}}\right] \tag{54}$$

Appendix C. Cost of other units

The cost of HXs, pumps and expanders can be evaluated by the equations of purchased and bare module cost, as posted in Table 11. The cost correlation of SE is reported as a function of the volumetric flow rate at the end of the expansion in m^3/s [43, 44]. The relative parameters and coefficients are indexed in Table 12 [31, 34, 45, 46]. The actual cost in the year 2018 needs to be converted from the cost of 2001 by introducing the *CEPCI* (Chemical Engineering Plant Cost Index) [47, 48].

Table 11. The cost estimating equations.

Item	Equation
Purchased cost of HX [32, 34, 49]	$log_{10}C_P = K_1 + K_2 log_{10}A + K_3 (log_{10}A)^2$
Purchased cost of pump and turbine [32, 34, 49]	$log_{10}C_P = K_1 + K_2 log_{10}W + K_3 (log_{10}W)^2$
Bare module cost of HX and pump [32, 34, 49]	$C_{BM} = C_P (B_1 + B_2 F_M F_P)$

Bare module cost of turbine [32, 34, 49]	$C_{BM,turbine} = C_P F_{BM} F_P$
Pressure factor [32, 34, 49]	$log_{10} F_P = C_1 + C_2 log_{10}(10p - 1) + C_3[log_{10}(10p - 1)]^2$
Cost of generator [32]	$C_{p,g} = 60(W_g)^{0.95}$
Cost correlation of SE [45, 47]	$C_{p,SE} = 3143.7 + 217423 V_{out}$
Cost in the year 2018 [43]	$C_{BM,2018} = C_{BM,2001} CEPCI_{2018}/CEPCI_{2001}$

Table 12. Values of constants for different components [31, 34, 45, 46].

Equipment	HX	Pump	Turbine
K_1	4.3247	3.3892	2.7051
K_2	-0.3030	0.0536	1.4398
K_3	0.1634	0.1538	-0.1776
C_1	0.0388	-0.3935	0
C_2	-0.11272	0.3957	0

C_3	0.08183	-0.00226	0
B_1	1.63	1.89	/
B_2	1.66	1.35	/
F_M	1.40	1.60	/
F_{BM}	/	/	3.40

References

[1] Mahmoudi A, Fazli M, Morad MR. A recent review of waste heat recovery by Organic Rankine Cycle. Appl Therm Eng 2018; 143: 660-675.

[2] Jiménez-Arreola M, Pili R, Magro FD, Wieland C, Rajoo S, Romagnoli A. Thermal power fluctuations in waste heat to power systems: An overview on the challenges and current solutions. Appl Therm Eng 2018; 134: 576-584.

[3] Magro FD, Jimenez-Arreola M, Romagnoli A. Improving energy recovery efficiency by retrofitting a PCM-based technology to an ORC system operating under thermal power fluctuations. Appl Energy 2017; 208: 972-985.

[4] Kim IS, Kim TS, Lee JJ. Off-design performance analysis of organic Rankine cycle using real operation data from a heat source plant. Energy Conv Manage 2017; 133: 284-291.

[5] Mazzi N, Rech S, Lazzaretto A. Off-design dynamic model of a real Organic Rankine Cycle system fuelled by exhaust gases from industrial processes. Energy 2015; 90: 537-551.

[6] Peralez J, Nadri M, Dufour P, Tona P, Sciarretta A. Control design for an automotive turbine Rankine cycle system based on nonlinear state estimation. In: 53rd IEEE Conference on Decision and Control at Los Angeles, December 15-17. 2014.

[7] Pili R, Romagnoli A, Spliethoff H, Wieland C. Techno-Economic Analysis of Waste Heat Recovery with ORC from Fluctuating Industrial Sources. Energy Proc 2017; 129: 503-510.

[8] Grelet V, Dufour P, Nadri M, Reiche T, Lemort V. Modeling and control of Rankine based waste heat recovery systems for heavy duty trucks. IFAC-Papers OnLine 2015; 28: 568-573.

[9] Steinmann W, Eck M. Buffer storage for direct steam generation. Sol Energy 2006; 80: 1277-1282.

[10] Concentrating Solar Power Thermal Storage System Basics. 2020. <https://www.energy.gov/eere/solar/articles/concentrating-solar-power-thermal-storage-system-basics> (accessed July 14, 2020).

[11] Relloso S, García E. Tower technology cost reduction approach after Gemasolar experience. Energy Proc 2015; 69: 1660-1666.

[12] Shouhang and EDF to Test s-CO_2 Cycle in Concentrated Solar Power. 2020. <http://www.cspfocus.cn/en/market/detail_1553.htm> (accessed July 14, 2020).

[13] König-Haagen A, Höhlein S, Brüggemann D. Detailed exergetic analysis of a packed bed thermal energy storage unit in combination with an Organic Rankine Cycle. Appl Therm Eng 2020; 165: 114583.

[14] Shu GQ, Zhao MR, Tian H, Wei HQ, Liang XY, Huo YZ, Zhu WJ. Experimental investigation on thermal OS/ORC (Oil Storage/Organic Rankine Cycle) system for waste heat recovery from diesel engine. Energy 2016; 107: 693-706.

[15] Li XY, Ma T, Liu J, Zhang H, Wang QW. Pore-scale investigation of gravity effects on phase change heat transfer characteristics using lattice Boltzmann method. Appl Energy 2018; 222: 92-103.

[16] Magro FD, Jimenez-Arreola M, Romagnoli A. Improving energy recovery efficiency by

retrofitting a PCM-based technology to an ORC system operating under thermal power fluctuations. Appl Energy 2017; 208: 972-985.

[17] Magro FD, Meneghetti A, Nardin G, Savino S. Enhancing energy recovery in the steel industry: Matching continuous charge with off-gas variability smoothing. Energy Conv Manage 2015; 104: 78-89.

[18] Magro FD, Savino S, Meneghetti A, Nardin G. Coupling waste heat extraction by phase change materials with superheated steam generation in the steel industry. Energy 2017; 137: 1107-1118.

[19] Yu XL, Li Z, Lu YJ, Huang R, Roskilly AP. Investigation of organic Rankine cycle integrated with double latent thermal energy storage for engine waste heat recovery. Energy 2019; 170: 1098-1112.

[20] Magro FD, Meneghetti A, Nardin G, Savino S. Enhancing energy recovery in the steel industry: Matching continuous charge with off-gas variability smoothing. Energy Conv Manage 2015; 104: 78-89.

[21] Li J, Gao GT, Kutlu C, Liu KL, Pei G, Su YH, Ji J, Riffat S. A novel approach to thermal storage of direct steam generation solar power systems through two-step heat discharge. Appl Energy 2019; 236: 81-100.

[22] Gao GT, Li J, Li PC, Cao JY, Pei G, Dabwan Y, Su YH. Design of steam condensation temperature for an innovative solar thermal power generation system using cascade Rankine cycle and two-stage accumulators. Energy Conv Manage 2019; 184: 389-401.

[23] Li J, Li PC, Gao GT, Pei G, Su YH, Ji J. Thermodynamic and economic investigation of a screw expander-based direct steam generation solar cascade Rankine cycle system using water as thermal storage fluid. Appl Energy 2017; 195: 137-151.

[24] Yu GP, Shu GQ, Tian H, Huo YZ, Zhu WJ. Experimental investigations on a cascaded steam-/organic-Rankine cycle (RC/ORC) system for waste heat recovery (WHR) from diesel engine. Energy Conv Manage 2016; 129: 43-51.

[25] Song J, Gu CW. Performance analysis of a dual-loop organic Rankine cycle (ORC) system with wet steam expansion for engine waste heat recovery. Appl Energy 2015; 156: 280-289.

[26] Li J, Li PC, Pei G, Alvi JZ, Ji J. Analysis of a novel solar electricity generation system using cascade Rankine cycle and steam screw expander. Appl Energy 2016; 165: 627-638.

[27] Karellas S, Leontaritis A, Panousis G, Bellos E, et al, E. Energetic and exergetic analysis of waste heat recovery systems in the cement industry. Energy 2013; 58: 147-156.

[28] Legmann H. Recovery of Industrial Heat in the Cement Industry by Means of the ORC-Process. IEEEIAS/PCA Cement Industry Techn. Conf., Jacksonville, FL, U.S., 2002.

[29] Steinmann, WD. EVA: Thermische Energiespeicher zur Verstromung diskontinuierlicher Abwärme: Forschungsbericht BWPLUS. Institute for Technical Thermodynamics. DLR. Stuttgart. 2010.

[30] Lemmon EW, Huber ML, McLinden MO. Refprop 8.0. NIST Standard reference database 23, version 8.0.

[31] Turton R, Bailie RC, Whiting WB. Analysis, synthesis and design of chemical processes (4th ed). Prentice Hall PTR, New Jersey. 2013.

[32] Cataldo F, Mastrullo R, Mauro AW, Vanoli GP. Fluid selection of organic Rankine cycle for low-temperature waste heat recovery based on thermal optimization. Energy 2014; 72: 159-167.

[33] HTRI Software. 2020. <http://www.htri.net; 2018> (accessed July 14, 2020).

[34] Yang MH, Yeh RH. Thermodynamic and economic performances optimization of an

organic Rankine cycle system utilizing exhaust gas of a large marine diesel engine. Appl Energy 2015; 149: 1-12.

[35] Li J. Gradual progress in the organic Rankine cycle and solar thermal power generation. In: Li J, editor. Structural optimization and experimental investigation of the organic rankine cycle for solar thermal power generation. Thesis, Springer. 2015.

[36] Tartière T, Astolfi M. A world overview of the organic Rankine cycle market. Energy Proc 2017; 129: 2-9.

[37] Perry RH, Chilton CH. Chemical Engineers' Handbook, (5th ed). McGraw-Hill, New York. 1973.

[38] FOB prices of steel products. <http://www.mysteel.net/> Shanghai Ganglian E-commerce Co., Ltd. (accessed July 14, 2020).

[39] Incropera FP, Dewit DP. Fundamentals of Heat and Mass Transfer, fifth ed., John Wiley and Sons, New York. 2002.

[40] Kern DQ. Process heat transfer. New York: McGraw-Hill. 1950.

[41] Gungor KE, Winterton RHS. Simplified general correlation for saturated flow boiling and comparisons for correlations with data. Chemical Engineering Research and Design 1987; 65: 148-56.

[42] Shah MM. A general correlation for heat transfer during film condensation inside pipes. International Journal of Heat and Mass Transfer 1979; 22: 547-56.

[43] Astolfi M. Techno-economic optimization of low temperature CSP systems based on ORC with screw expanders. Energy Proc 2015; 69: 1100-1112.

[44] PÉREZ BP. Thermo-economic assessment of small-scale organic Rankine cycle for low-grade industrial waste heat recovery based on an experimental application. Doctoral Thesis,

Universitat Jaume. July 2017. Chapter IV p. 110.

[45] Shu GQ, Liu P, Tian H, Wang X, Jing DZ. Operational profile based thermal-economic analysis on an Organic Rankine cycle using for harvesting marine engine's exhaust waste heat. Energy Conv Manage 2017; 146: 107-123.

[46] Li J, Hu SZ, Yang FB, Duan YY, Yang Z. Thermo-economic performance evaluation of emerging liquid-separated condensation method in single-pressure and dual-pressure evaporation organic Rankine cycle systems. Appl Energy 2019; 256: 113974.

[47] Li TL, Meng N, Liu J, Zhu JL, Kong XF. Thermodynamic and economic evaluation of the organic Rankine cycle (ORC) and two-stage series organic Rankine cycle (TSORC) for flue gas heat recovery. Energy Conv Manage 2019; 183: 816-829.

[48] 2018 CEPCI UPDATES: MAY (PRELIM.) AND APRIL (FINAL). 2020. <https://www.chemengonline.com/2018-cepci-updates-may-prelim-and-april-final> (accessed July 14, 2020).

[49] Zhang C, Liu C, Wang SK, Xu XX, Li QB. Thermo-economic comparison of subcritical organic Rankine cycle based on different heat exchanger configurations. Energy 2017; 123: 728-741.

Nomenclature		Q	heat, kJ
A	HX area, m^2	Re	Reynolds number
a	half long axis, mm	S	allowable stress, MPa
b	half short axis, mm	T	temperature, °C
Bo	boiling number	t	thickness, mm

C	cost, \$ /coefficient	U	heat transfer coefficient
c_p	specific heat capacity, kJ/(kg·K)	u	flow velocity, m/s
D	diameter, mm	V	volume, m^3
d	hydraulic diameter, m	W	work, kW
E	welded joint efficiency	Y	yield, \$
f	Darcy resistance coefficient	α	convection heat transfer
G	mass flux, kg/(m^2·s)		coefficient, W/ (m^2·K)
H	height, mm	ε	device efficiency
h	enthalpy, kJ/kg /	η	efficiency
	height of head, mm	λ	thermal conductivity, W/(m·K)
i	internal	υ	kinematic viscosity, m^2/s
K	geometric factor	ρ	density, kg/m^3
M	mass, kg	τ	time, h
m	mass flow rate, kg/s	χ	quality
P	cost per kilogram, \$/kg		
p	pressure, MPa	***Abbreviation***	
Pr	Prandtl number	ASME	American Society of
	Mechanical Engineers	*cascade*	cascade system
CA	corrosion allowance	*cy*	cylinder
CEPCI	Chemical Engineering Plant	*elec*	electricity
	Cost Index	*g*	generator
EPP	equivalent payback period	$head$	elliptical head

HTA	high temperature accumulator	*in*	inlet
HX	heat exchanger	*l*	liquid
LTA	low temperature accumulator	*loss*	power loss
NIC	normalized investment cost	*M*	material
ORC	organic Rankine cycle	*max*	maximum
P	pump	*min*	minimum
PCM	phase change material	*net*	net power
RC	steam Rankine cycle	*OT*	ORC turbine
RC-ORC	steam-organic Rankine cycles	*out*	outlet
SE	screw expander	*p*	pressure / pump / purchased
TES	thermal energy storage	*s*	isentropic / single-phase
		sl	saturated liquid
Subscript		*ss*	saturated steam/ single-stage
1…22	number	*steel*	steel
b	boiling / binary	*t*	thermal
BM	bare module	*v*	vapor
c	condensation	*w*	water